CEAS-GNC-2022-035

CEAS EuroGNC 2022
"Conference on Guidance, Navigation and Control"
3-5 May 2022 @ Technische Universität Berlin, Germany

Nonlinear Model Following Control Design for a Hypersonic Waverider Configuration

Johannes Autenrieb Research Scientist, DLR, Institute of Flight Systems, Department of Flight Dynamics and Simulation, 38108, Braunschweig, Germany. johannes.autenrieb@dlr.de

Nicolas Fezans Scientific Advisor, DLR, Institute of Flight Systems, Department of Flight Dynamics and Simulation, 38108, Braunschweig, Germany. nicolas.fezans@dlr.de

ABSTRACT

The German Aerospace Center (DLR) is currently studying and developing key technologies to implement autonomous hypersonic flight systems into different mission scenarios. One configuration type of higher interest for civil and military purposes is the hypersonic glide vehicle (HGV) waverider concept. Such HGVs are operating over highly widespread flight envelopes and are posing complex flight dynamic characteristics. This paper presents a generic hypersonic glide vehicle concept developed by the DLR and proposes a nonlinear flight control architecture that is based on the idea of the nonlinear dynamic inversion and nonlinear model following control methodologies. The proposed control scheme is designed to adequately and robustly handle the system dynamics of the over-actuated vehicle. The approach is first discussed, and the performance of the suggested control laws is later investigated via simulations of a high-fidelity nonlinear flight dynamic model in the nominal case and under the existence of parameter uncertainties and disturbances. The presented results demonstrate that the proposed approach provides significant benefits for the robust control of the hypersonic system.

Keywords: Nonlinear Flight Control; Nonlinear Dynamic Inversion; Nonlinear Model Following Control; Hypersonic Glide Vehicles; Waverider; Flight Mechanics

Nomenclature

The notation convention used in this paper is widely based on the notation presented in the ISO 1151 standard series for flight mechanical quantities part one and part two [1, 2].

H	=	Altitude
m, I	=	Mass and Inertia matrix
L_A, Y_A	=	Aerodynamic lift force and side force
L, M, N	=	External moments in body axes
p_K, q_K, r_K	=	Roll, pitch, yaw rate in body axes w.r.t. the inertial system
X, Y, Z	=	External forces in body axes
u_K, v_K, w_K	=	Translational velocities in body axes w.r.t. the inertial system
W	=	Weight force
γ	=	Flight path angle
χ	=	Flight path azimuth angle
Φ, Θ, Ψ	=	Euler angles of roll, pitch, and yaw
μ, β, α	=	Flight path roll angle, angle of attack and sideslip angle

1 Introduction

In the last years, hypersonic glide vehicles (HGVs) have been increasingly the subject of research and development efforts of both academia and the industry. This emerging class of vehicle possesses the ability to be applied in the civil and military sector. The German Aerospace Center (DLR) is currently studying the physical limitations and performance of autonomous hypersonic flight systems in different mission scenarios. Well-designed autopilots are compulsory for all autonomously operating flight vehicles. The mentioned systems stabilize the vehicle and ensure good tracking behavior regarding an online or offline computed trajectory to reach the desired location. Particularly for the application in hypersonic vehicles, the implemented guidance and control systems need to adequately and robustly handle the complex physical effects over large flight envelopes under the presence of model uncertainties and inaccurate model assumptions. One promising control approach which is naturally able to handle highly nonlinear systems is the nonlinear dynamic inversion (NDI) control methodology.

NDI has been successfully applied and tested for flight control systems of different aerial vehicle classes in recent years. In [3] the authors successfully applied cascaded NDI feedback controllers for the autonomous attitude control of a hypersonic re-entry vehicle and in [4] for the control augmentation system of a supermaneuverable aircraft. Both discussed approaches use a time-scale separation for improved robustness of the continuous feedback linearization scheme [5]. Even though the approaches show promising results, the established control systems mutually rely on the implemented linear feedback controllers for good tracking performance and stability augmentation. Such a control structure makes it tedious to tune the controllers and consequently increases the possibility of high-gain solutions, leading to decreased robustness properties and closed-loop characteristics. The flight control architecture presented in this paper uses the fundamental ideas presented in [3, 4] for feedback control but enhances the structures with a feedforward signal based on the idea of a nonlinear model following control (NMFC) approach [6]. For this, a second-order model reference system and known kinematic relationships are combined to fundamentally separate the command tracking task from the stability augmentation task of the controllers.

In this paper, an overview of the vehicle and its mission design is given. Following this, the nonlinear mathematical model and relevant flight dynamic relationships are presented and discussed. Further, the established nonlinear flight control system design is introduced and discussed. Finally, an example of a time simulation is used to demonstrate the control performance and the robustness of the proposed control system.

2 Hypersonic glide vehicle modeling

2.1 The DLR GHGV-2 Concept

The Generic Hypersonic Glide Vehicle 2 (GHGV-2), which is presented in this section, has been designed by a multi-disciplinary development group of DLR. The GHGV-2 concept was developed to deeply investigate hypersonic glide vehicles' physical capabilities, limitations and their future impact on operations in the civil and military domains. The developed vehicle is displayed in Fig. 1a in an overall view and in Fig. 1b in a sectional view with relevant sub-systems, such as the thermal protection system (TPS), guidance, navigation & control system (GNC), battery, and actuators. The flight vehicle is based on the aerodynamical foundations of waveriders and is designed to improve lift-to-drag ratios within operations in high Mach number regimes [7].

For the currently investigated use-cases, it is expected that the GHGV-2 is placed on the head section of a two-stage boost-rocket. Once launched, the launch vehicle is planned to carry the HGV to an altitude of approximately 100 km. When the target height is reached, the hypersonic glide vehicle decouples from

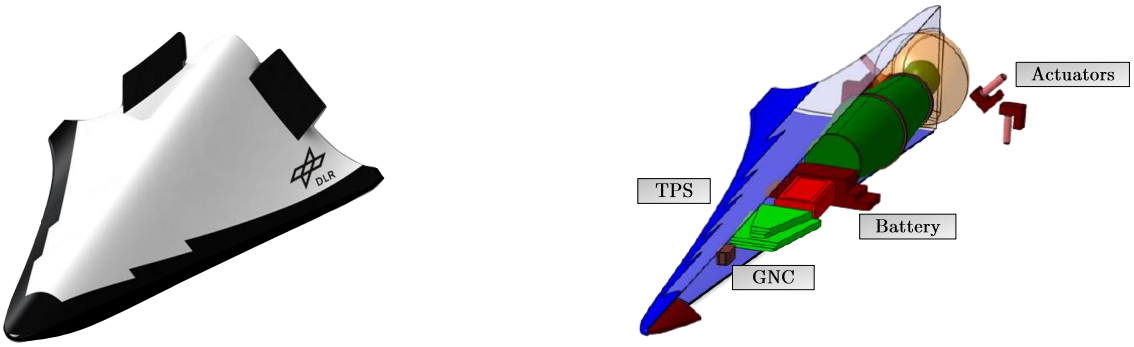

(a) External view on the GHGV-2 **(b) Sectional view of the GHGV-2**

Fig. 1 The DLR Generic Hypersonic Glide Vehicle Concept [7].

the head section and initiates a free flight period. After a ballistic reentry phase, the vehicle enters the atmospheric glide flight, in which the system typically cruises with maintaining the $(L/D)_{max}$ related flight path angle γ. For the operations in altitudes in which no sufficient aerodynamical control authority can be guaranteed, the vehicle is equipped with additional thrusters as control effectors. Once the reentry phase is successfully passed, four integrated fins (two on the upper and two on the lower side) can be used for the aerodynamical attitude control of the vehicle. As this description suggests, the control effectiveness of the implemented control effectors is highly dependent of the current flight phase of the flight vehicle. Since the developed flight control system is focusing on pure attitude control goals (three degrees of freedom) and based on the number of available control effectors in both flight phases (in both cases at least four control effectors), the vehicle can be regarded as over-actuated. For such a system, the application of suitable control allocation algorithms within the later discussed flight control design is required.

2.2 Nonlinear flight dynamics

The modeled nonlinear flight dynamics of the HGV are based on classical Newtonian mechanics, in which the vehicle is assumed as a rigid body. Fig. 2 displays the components of the total external forces X, Y, Z and the total external moments L, M, N expressed in the body-fixed frame of the vehicle. For the investigated case, only the aerodynamic and gravitational forces and moments are considered relevant during the regarded reentry and glide phase since hypersonic glide vehicles are commonly unpropelled during those mission stages.

The generalized equations of motion of an aerial vehicle are presented for the translational movement in Eq. (1) and for the rotational movement in Eq. (2).

$$\begin{bmatrix} X \\ Y \\ Z \end{bmatrix} = m \begin{bmatrix} \dot{u}_K \\ \dot{v}_K \\ \dot{w}_K \end{bmatrix} + m \begin{bmatrix} p_K \\ q_K \\ r_K \end{bmatrix} \times \begin{bmatrix} u_K \\ v_K \\ w_K \end{bmatrix} \qquad (1)$$

$$\begin{bmatrix} L \\ M \\ N \end{bmatrix} = I \begin{bmatrix} \dot{p}_K \\ \dot{q}_K \\ \dot{r}_K \end{bmatrix} + \begin{bmatrix} p_K \\ q_K \\ r_K \end{bmatrix} \times I \begin{bmatrix} p_K \\ q_K \\ r_K \end{bmatrix} \qquad (2)$$

The kinematic relationship connecting the derivatives of the flight-path bank angle μ_K, the angle of attack α_K and the sideslip angle β_K to the body-fixed rotational rates p_K, q_K, r_K and the corresponding derivatives of the flight path angle γ and χ can be stated as [8, 9]:

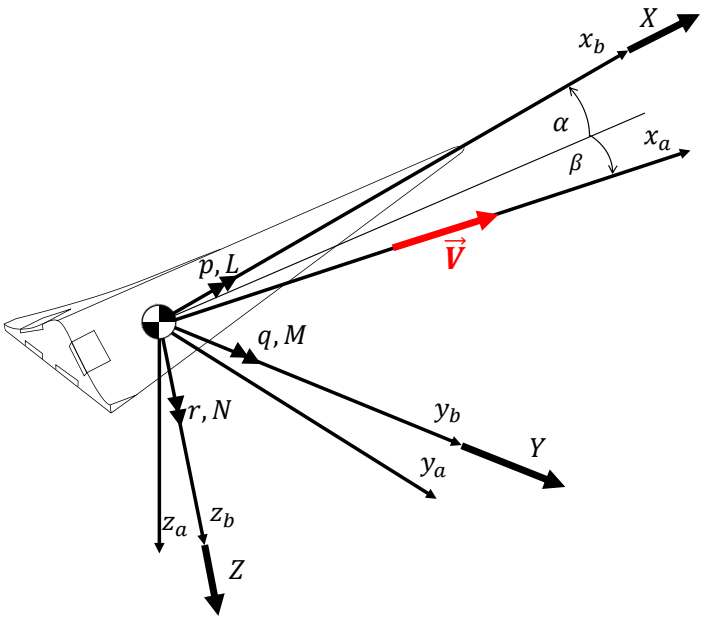

Fig. 2 Sketch of external forces and moments attacking on the GHGV-2 concept.

$$\begin{bmatrix}\dot{\mu}_K\\ \dot{\alpha}_K\\ \dot{\beta}_K\end{bmatrix} = T_1\begin{bmatrix}p_K\\ q_K\\ r_K\end{bmatrix} + T_2\begin{bmatrix}\dot{\gamma}\\ \dot{\chi}\end{bmatrix} = \begin{bmatrix}\frac{\cos\alpha_K}{\cos\beta_K} & 0 & \frac{\sin\alpha_K}{\cos\beta_K}\\ -\cos\alpha_K\tan\beta_K & 1 & -\sin\alpha_K\tan\beta_K\\ \sin\alpha_K & 0 & -\cos\alpha_K\end{bmatrix}\begin{bmatrix}p_K\\ q_K\\ r_K\end{bmatrix} + \begin{bmatrix}\cos\mu_K\tan\beta_K & \sin\gamma + sin\mu\tan\beta_K\cos\gamma\\ -\frac{\cos\mu_K}{\cos\beta_K} & -\frac{\sin\mu_K\cos\gamma}{\cos\beta_K}\\ -\sin\mu_K & \cos\mu_K\cos\gamma\end{bmatrix}\begin{bmatrix}\dot{\gamma}\\ \dot{\chi}\end{bmatrix} \tag{3}$$

For the kinematic relationship presented in Eq. (3), the influences of the time derivatives of the flight path angle γ and χ can be reformulated and expressed as functions of the externally attacking weight force W, aerodynamic lift force L_A and aerodynamic side force Y_A described in the inertial axes:

$$\begin{bmatrix}\dot{\mu}_K\\ \dot{\alpha}_K\\ \dot{\beta}_K\end{bmatrix} = T_1\begin{bmatrix}p_K\\ q_K\\ r_K\end{bmatrix} + \left(\frac{1}{mV}\right)T_3\begin{bmatrix}-W\\ L_A\\ Y_A\end{bmatrix} = \begin{bmatrix}\frac{\cos\alpha_K}{\cos\beta_K} & 0 & \frac{\sin\alpha_K}{\cos\beta_K}\\ -\cos\alpha_K\tan\beta_K & 1 & -\sin\alpha_K\tan\beta_K\\ \sin\alpha_K & 0 & -\cos\alpha_K\end{bmatrix}\begin{bmatrix}p_K\\ q_K\\ r_K\end{bmatrix} + \left(\frac{1}{mV}\right)\begin{bmatrix}\cos\gamma\cos\mu_K\tan\beta_K & \tan\gamma\sin\mu_K + \tan\beta_K & \tan\gamma\cos\mu_K\cos\beta_K\\ \frac{\cos\gamma\cos\mu_K}{\cos\beta_K} & -\frac{1}{\cos\beta_K} & 0\\ \cos\gamma\sin\mu_K & 0 & \cos\beta_K\cos\gamma\end{bmatrix}\begin{bmatrix}-W\\ L_A\\ Y_A\end{bmatrix} \tag{4}$$

Eq. (3) and Eq. (4) express a general kinematic relationship that also stays valid for cases in which the described aerial vehicle operates in windy conditions. Nevertheless, to simplify the notation for this paper, the nonexistence of wind is assumed. In that considered case, the inertial axes denoted by the index K correspond with the aerodynamic axes denoted by the index a. In order to further simplify

the used notation, in the rest of the paper, the body-rate rate vector, which is described in the inertial axes denoted by the index K, is used without the corresponding index. The mentioned assumptions and simplifications lead to the following simplified notation:

$$\begin{bmatrix} \mu_K \\ \alpha_K \\ \beta_K \end{bmatrix} = \begin{bmatrix} \mu_a \\ \alpha_a \\ \beta_a \end{bmatrix} = \begin{bmatrix} \mu \\ \alpha \\ \beta \end{bmatrix} \quad (5) \qquad \begin{bmatrix} \gamma_a \\ \chi_a \end{bmatrix} = \begin{bmatrix} \gamma \\ \chi \end{bmatrix} \quad (6) \qquad \begin{bmatrix} p_K \\ q_K \\ r_K \end{bmatrix} = \begin{bmatrix} p \\ q \\ r \end{bmatrix} \quad (7)$$

The lift force L_A and the side force Y_A are computed based on a provided high-fidelity nonlinear aerodynamic database of the HGV; see [10] for more details. The aerodynamic model is formulated as a function of the angle of attack α, sideslip angle β, Mach number Ma, altitude H and the control deflection vector δ. An independent computation of the control effectiveness and their overall influences on the vehicle's dynamics is provided for all aerodynamic surfaces. At the current point, the influences of the flaps on the vehicle's dynamics are assumed to be linear, but it is also planned to consider the nonlinear effects of the flap deflections in future steps of the research process.

3 Integrated nonlinear flight control design

For the GHGV-2, a nonlinear model-following-control system was designed and integrated. The overall structure of the established controller is displayed in Fig. 3. The architecture uses a second-order reference model (RM) system to filter the command input vector $(\mu_{cmd}, \alpha_{cmd}, \beta_{cmd})^T$ and shape the desired reference signal vector $(\mu_{ref}, \alpha_{ref}, \beta_{ref})^T$. The generated reference signals are the filtered commands and the corresponding first and second derivatives of the desired model response. The RM comprises further knowledge of physical limitations on the different time scales and protects the controllers of unworkable reference signals. Such limits can originate in defined general structural and thermal load limits that the vehicle should not exceed. Other influences that can be regarded within the MR limitations are that the actuator capabilities of vehicles operating in high-speed regimes can significantly vary over the flight envelope due to external factors, such as high dynamical pressure and thermal influences acting on the fins. Such influences can limit the vehicle's actuation capacity and restrict the maximal achievable rate of changes that the integrated control effectors can provide.

The generalized control task can be decomposed into two main control tasks: tracking and regulation. The first task is taken over by transforming the computed higher-order derivatives of the feed-forward signals based on known systems kinematics and dynamics. The second task is taken over by a control feedback path to handle uncertainties and external disturbances. For the feedback control, a cascaded time-scale separated nonlinear dynamic inversion control system is implemented. Time-scale separation is a method that takes the modeled flight dynamics and hence the physical process into account [5]. From a physical point of view, a moment needs to act on the system to change the vehicle's attitude. In the following time step, this moment consequently leads to a change in the angular rates, while the attitude itself would remain the same for the corresponding time step. Finally, the altered angular rates lead to a desired attitude change in the next time step. Since these physical properties are observed in reality, it has been suggested to establish a control method that takes this behavior to account in order to achieve higher control robustness regarding model uncertainties. For flight control systems commonly, a two-loop approach with distinct cascaded outer (attitude control) and inner (body-rates control) loop controllers is suggested to handle the slow and fast dynamics of the aerial vehicles. In order to fulfill the assumption of time-scale separation for such two-loop controllers, it needs to be ensured that the bandwidth of the actuators is much higher than the bandwidth of the implemented inner loop controllers since the influences of the actuator dynamics on the flight states are commonly neglected within the feedback

linearization of the controllers. Further, it also needs to be ensured that after the gain tuning procedure of the controllers, the inner loop controller bandwidth is significantly higher (experiences are suggesting at least 10x larger) than the outer loop controller bandwidth in order to fully benefit from the promised increased robustness of the time-scale separation approach.

Even though the described control approach is commonly used in flight control, it also comes with disadvantages. One major disadvantage is that unstable inner loop controllers would consequently lead to overall unstable closed-loop behavior. Further, the gain tuning and the clearance processes for the developed flight control system are more complex and time-consuming due to the broader interconnectedness between the different physical properties and parameters. The following section presents and discusses further the overall NDI flight control system and its relevant sub-systems proposed for the attitude control of the GHGV-2.

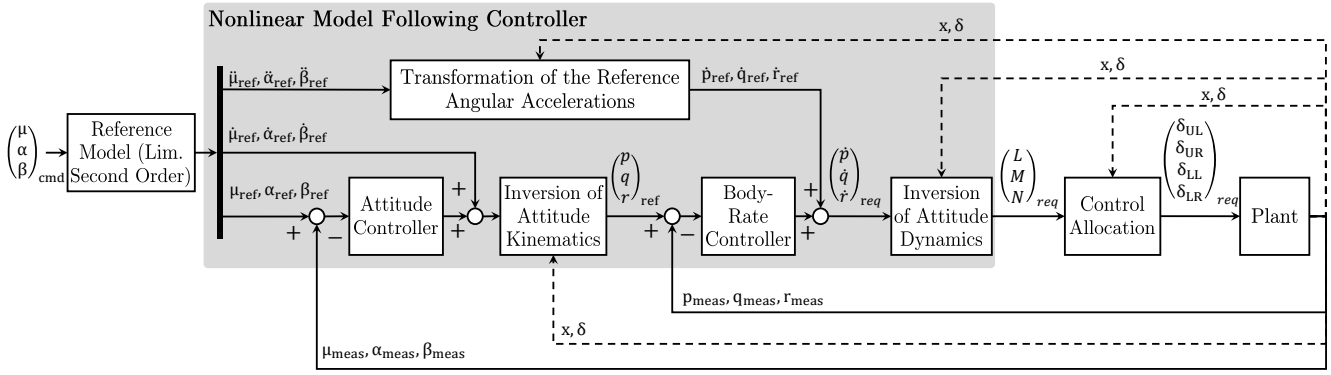

Fig. 3 Overview on proposed nonlinear model following control architecture for the GHGV-2.

3.1 NDI-based attitude feedback control design

A cascaded nonlinear dynamic inversion feedback controller, with distinct linear controllers for the attitude and rate control, is implemented for good stability augmentation and disturbance rejection capabilities of the vehicle. The integrated cascaded feedback control approach is based on the idea of timescale separated nonlinear dynamic inversion systems presented in [3, 4], but is adapted to match the technical realization of the controlled generic hypersonic glide vehicle.

The input of the linear outer-loop controllers is the time-dependent tracking error vector $(e_\mu, e_\alpha, e_\beta)^T$, which is computed based on the state measurements and the obtained tracking commands of the RM (as explained in Sect. 3.3). The implemented linear controllers regulate the system's error dynamics by computing the derivatives of the aerodynamic angles needed to eliminate the attitude control error:

$$\begin{bmatrix} \Delta\dot{\mu} \\ \Delta\dot{\alpha} \\ \Delta\dot{\beta} \end{bmatrix} = K_{\mu\alpha\beta} \begin{bmatrix} e_\mu \\ e_\alpha \\ e_\beta \end{bmatrix} = \begin{bmatrix} K_\mu & 0 & 0 \\ 0 & K_\alpha & 0 \\ 0 & 0 & K_\beta \end{bmatrix} \left(\begin{bmatrix} \mu_{ref} \\ \alpha_{ref} \\ \beta_{ref} \end{bmatrix} - \begin{bmatrix} \mu_{meas} \\ \alpha_{meas} \\ \beta_{meas} \end{bmatrix} \right) \tag{8}$$

The required first-order time derivatives of the aerodynamic angles are obtained by combining the reference model output vector $(\dot{\mu}_{ref}, \dot{\alpha}_{ref}, \dot{\beta}_{ref})^T$ and the generated feedback control signal vector $(\Delta\dot{\mu}, \Delta\dot{\alpha}, \Delta\dot{\beta})^T$.

$$\begin{bmatrix} \dot{\mu}_{req} \\ \dot{\alpha}_{req} \\ \dot{\beta}_{req} \end{bmatrix} = \begin{bmatrix} \dot{\mu}_{ref} \\ \dot{\alpha}_{ref} \\ \dot{\beta}_{ref} \end{bmatrix} + \begin{bmatrix} \Delta\dot{\mu} \\ \Delta\dot{\alpha} \\ \Delta\dot{\beta} \end{bmatrix} \tag{9}$$

By using the presented angular kinematics from Eq. (8) for the inversion of the regarded dynamics, the command input for the inner-loop controllers can be computed as follows:

$$\begin{bmatrix} p_{ref} \\ q_{ref} \\ r_{ref} \end{bmatrix} = T_1^{-1} \left(\begin{bmatrix} \dot{\mu}_{req} \\ \dot{\alpha}_{req} \\ \dot{\beta}_{req} \end{bmatrix} - \left(\frac{1}{mV} \right) T_3 \begin{bmatrix} -W \\ L_A \\ Y_A \end{bmatrix} \right) \tag{10}$$

The input of the linear inner-loop controller is the time-dependent tracking error vector $(e_r, e_q, e_r)^T$, which is computed based on the state measurements and the obtained commands of the angular kinematics inversion step. The implemented linear controllers regulate the system's error dynamics by computing the virtual control commands needed to eliminate the rate control error:

$$\begin{bmatrix} \Delta\dot{p} \\ \Delta\dot{q} \\ \Delta\dot{r} \end{bmatrix} = K_{pqr} \begin{bmatrix} e_p \\ e_q \\ e_r \end{bmatrix} = \begin{bmatrix} K_p & 0 & 0 \\ 0 & K_q & 0 \\ 0 & 0 & K_r \end{bmatrix} \left(\begin{bmatrix} p_{ref} \\ q_{ref} \\ r_{ref} \end{bmatrix} - \begin{bmatrix} p_{meas} \\ q_{meas} \\ r_{meas} \end{bmatrix} \right) \tag{11}$$

By using the kinematic relationship presented in Eq. (3), the computed rotational acceleration vector $(\Delta\dot{p}, \Delta\dot{q}, \Delta\dot{r})^T$ is additionally augmented with the feedforward signal vector $(\dot{p}_{ref}, \dot{q}_{ref}, \dot{r}_{ref})^T$ from the command filter, which is explained in Sect. 3.2 in more detail.

$$\begin{bmatrix} \dot{p}_{req} \\ \dot{q}_{req} \\ \dot{r}_{req} \end{bmatrix} = \begin{bmatrix} \dot{p}_{ref} \\ \dot{q}_{ref} \\ \dot{r}_{ref} \end{bmatrix} + \begin{bmatrix} \Delta\dot{p} \\ \Delta\dot{q} \\ \Delta\dot{r} \end{bmatrix} \tag{12}$$

After the augmentation, the signals are transformed into the required moments $\vec{Q}_{req}$ using the following relationship:

$$\vec{Q}_{req} = \begin{bmatrix} L_{req} \\ M_{req} \\ N_{req} \end{bmatrix} = I \begin{bmatrix} \dot{p}_{req} \\ \dot{q}_{req} \\ \dot{r}_{req} \end{bmatrix} + \begin{bmatrix} p \\ q \\ r \end{bmatrix} \times I \begin{bmatrix} p \\ q \\ r \end{bmatrix} \tag{13}$$

3.2 Nonlinear model following control

The integrated nonlinear flight control architecture is designed as a nonlinear model following controller. The fundamental concept of this control strategy is to separate the command tracking tasks from the regulation tasks of the flight control system by using knowledge of the system dynamics and kinematic relationships. As explained priorly, a second-order RM applied to filter the command inputs and shape the desired reference signals. The reference model incorporates further knowledge of physical constraints on the different time scales and protects the controllers of unworkable reference signals. As long as the system is operating within its defined boundaries, the incoming commands from the guidance system $(\mu_{cmd}, \alpha_{cmd}, \beta_{cmd})^T$ are shaped by second-order transfer functions which can be described in the following form:

$$G_{ref}(s) = \frac{\omega_{ref}^2}{s^2 + 2D_{ref}\omega_{ref}s + \omega_{ref}^2} \tag{14}$$

The eigenfrequency ω_{ref} and the damping ration D_{ref} of the presented transfer function can be chosen such that the desired system response behavior can be imposed on the vehicle. Besides the desired angular state reference signals, the reference models also generate the first and second order derivatives of the desired response. These signals are used for feedforwarding control signals directly to the inner and outer loop controllers, increasing the system's tracking performance. This enables to partially decompose the command tracking tasks from the regulation tasks of the feedback control system and hence eases up the tuning and consequently decreases the possibility of high-gain solutions. As described previously, the first-order time derivative vector of the shaped reference responses $(\dot{\mu}_{ref}, \dot{\alpha}_{ref}, \dot{\beta}_{ref})^T$ are feedforwarded to the inner-loop inversion of the attitude kinematics. The second-order time derivatives of the shaped reference responses $(\ddot{\mu}_{ref}, \ddot{\alpha}_{ref}, \ddot{\beta}_{ref})^T$ are used for feedforward purposes by using the known kinematic relationship presented in Eq. (3). Following the NDI methodology discussed earlier, the regarded dynamic relationship needs to be further derived to obtain the needed input-output connection that matches the second-order derivatives of the aerodynamic angular reference signals with the virtual control command vector $(\dot{p}_{ref}, \dot{q}_{ref}, \dot{r}_{ref})^T$. The final feedforward virtual control command signal is described as [9]:

$$\begin{bmatrix} \dot{p}_{ref} \\ \dot{q}_{ref} \\ \dot{r}_{ref} \end{bmatrix} = T_1^{-1} \left[\begin{pmatrix} \ddot{\mu}_{ref} \\ \ddot{\alpha}_{ref} \\ \ddot{\beta}_{ref} \end{pmatrix} - \dot{T}_1 \begin{pmatrix} p \\ q \\ r \end{pmatrix} - \dot{T}_2 \begin{pmatrix} \dot{\gamma} \\ \dot{\chi} \end{pmatrix} - T_2 \begin{pmatrix} \ddot{\gamma} \\ \ddot{\chi} \end{pmatrix} \right] \tag{15}$$

3.3 Control Allocation

As described in Sect. 2.1, the application of suitable control allocation algorithms for the over-actuated GHGV-2 is required. Although the presented vehicle is over-actuated in both exoatmospheric and endoatmospheric flight regimes, only the endoatmospheric flight phase is further regarded in the following discussion, due to the brevity of this paper. Accordingly, only the control allocation problem in which the integrated fins are available as redundant control effectors is addressed. Fig. 4 shows the available control effectors with the connected deflections of the upper left fin δ_{UL}, upper right fin δ_{UR}, lower left fin δ_{LL} and lower right fin δ_{LR} for the described case.

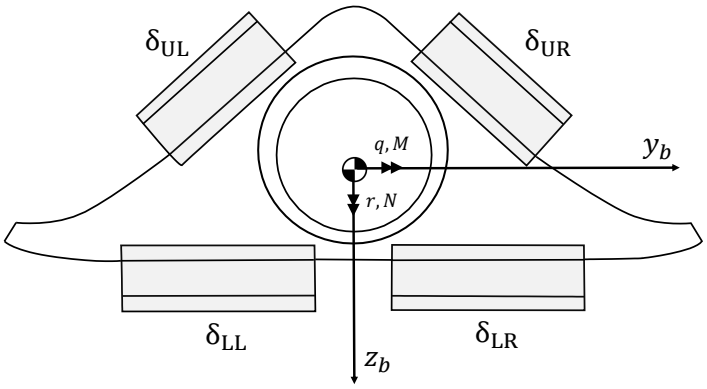

Fig. 4 Conceptual sketch with rear view on GHGV-2 and available control effectors during endoatmospheric operations.

To solve the control allocation problem of the over-actuated flight vehicle, the control effectiveness matrix B is needed. The matrix describes the influences of all available control effectors on the balance of moment around the distinct body-fixed axes of the vehicle.

$$B = \begin{pmatrix} \frac{\partial L}{\partial \delta_{UL}} & \frac{\partial L}{\partial \delta_{UR}} & \frac{\partial L}{\partial \delta_{LL}} & \frac{\partial L}{\partial \delta_{LR}} \\ \frac{\partial M}{\partial \delta_{UL}} & \frac{\partial M}{\partial \delta_{UR}} & \frac{\partial M}{\partial \delta_{LL}} & \frac{\partial M}{\partial \delta_{LR}} \\ \frac{\partial N}{\partial \delta_{UL}} & \frac{\partial N}{\partial \delta_{UR}} & \frac{\partial N}{\partial \delta_{LL}} & \frac{\partial N}{\partial \delta_{LR}} \end{pmatrix} \tag{16}$$

$$\vec{\delta}^T = \begin{bmatrix} \delta_{UL} & \delta_{UR} & \delta_{LL} & \delta_{LR} \end{bmatrix}^T \tag{17}$$

In reality, such a matrix is highly nonlinear since it is dependent on a wide variety of parameters, such as the current flight state, atmospheric conditions, and the control inputs themselves. Nevertheless, for the simplification of the problem, the last-mentioned nonlinear effect is often neglected since it is assumed that those effects are not highly significant on the control authority. In order to cope with the other mentioned nonlinear effects, the B matrix is continuously re-computed by using an onboard plant model and sensor measurements but is then assumed constant for each time step. In the simplest case, the control allocation problem of the GHGV-2 can be solved by using linear algebra. In order to do so, further nonlinearities of the control allocation problem, such as the deflection limits $\vec{\delta}_{min/max}$ and rate limits $\dot{\vec{\delta}}_{min/max}$ of the actuators, need to be neglected. Under these assumptions, the control allocation problem of the flight vehicle can be solved by using a Moore-Penrose pseudoinverse in the following form:

$$\vec{\delta}_{req} = B^{+}\vec{Q}_{req} = B^T[BB^T]^{-1}\vec{Q}_{req} \tag{18}$$

However, especially for vehicles with novel control concepts and systems that operate in highly nonlinear flight regimes, the presented approach could reach its limits and consequently cause severe problems during the operation. Further, it is often required to manage the available control effectors in a way that constraints, such as concerning finite resources (e.g., thrusters as control effectors) and the possible existence of corrupted control effectors, are considered during operation. Therefore it was decided to formulate the control allocation problem of the GHGV-2 as a constrained optimization problem. In this way, the mentioned operational constraints, such as deflection limits $\vec{\delta}_{min/max}$ and rate limits $\dot{\vec{\delta}}_{min/max}$, of the actuators can be considered. In the current state of the project, further constraints are not regarded in the optimization. However, future steps are planned to enhance the optimization problem with a weighted performance index that takes degraded control authority and restricted resources to account. The resulting constrained optimization problem of the control allocation algorithm can be stated as:

$$\begin{aligned} &\underset{\delta \in \mathbb{R}^{n_u}}{\arg\min} && \|B\vec{\delta} - \vec{Q}_{req}\|_2 \\ &\text{subject to} && \vec{\delta}_{min} \leq \vec{\delta} \leq \vec{\delta}_{max}, \\ & && \dot{\vec{\delta}}_{min} \leq \dot{\vec{\delta}} \leq \dot{\vec{\delta}}_{max} \end{aligned} \tag{19}$$

With n_u being the number of available control effectors, the here formulated least-square optimization problem leads to the minimization of the difference between the requested moment vector $\vec{Q}_{req}$ and the achievable control input moment vector $B\vec{\delta}$ in the l_2 norm sense and with the control deflection vector $\vec{\delta}$ complying with position and rate limits. By using the l_2 norm, the optimization algorithm tends to distribute the incoming command on all control effectors evenly, provided that no limits are reached, and the control effectors have the same effectiveness. By using different norms, different solutions can be obtained. For example, by using the l_1 norm, the optimization algorithm would try to use as few control inputs as possible to satisfy the requested moment vector [11]. However, the latter approach tends more

to undesired saturation effects of the control effectors. The solution of the introduced optimization problem is searched using an active set algorithm that is based on a quadratic programming method in which the actuator limits are considered using Lagrange multipliers [12]. The starting point $\vec{\delta}_0$ of the active set optimization procedure corresponds in the first time step with the trim solution of the initial flight state and afterwards with the commanded control deflections of the previous time step. For cases in which one parameter of $\vec{\delta}_0$ is not within the set boundaries of the deflection limits $\vec{\delta}_{min}$ or $\vec{\delta}_{max}$ the input is neglected, and the corresponding overstepped deflection limit entry of the defined deflection limit vector is used.

4 Simulation Results

A simulation-based controller evaluation process was carried out to examine the proposed controller design. It needs to be addressed that specific hypersonic waverider configurations, including the presented vehicle, tend to unstable open-loop behavior in the longitudinal and lateral-directional motion characteristics [13, 14]. Combined with the complex flight physics in hypersonic operations and non-trivial cross-coupling effects for both the longitudinal and lateral-directional flight control properties, a large field for in-depth flight dynamical and control performance analysis is of higher interest for research activities. Nevertheless, the authors decided that only a selected part of the tracking and regulation performance assessment of the integrated nonlinear model following control architecture is presented in this paper. In the following analysis, an exemplary angle of attack α_{cmd} doublet trajectory is given into the flight control system, in two cases: with and without the existence of model uncertainties. The high-fidelity model and the applied aerodynamic dataset used for the time simulations are provided in a MATLAB/Simulink environment specifically developed for the control design of hypersonic flight vehicles; see [10] for more details. The integrated actuators of the employed control fins are modeled as second-order systems, which include preset deflection angle, rate, and acceleration limits. For this paper, the authors decided to concentrate on the proposed controller's robustness assessment exclusively regarding real parametric uncertainties; influences on the controller due to sensor inaccuracies are not regarded. Consequently, perfect and undelayed measurements of the flight vehicle's states were assumed within the presented and discussed results of the simulation-based assessment. In-depth assessments with regards to sensor inaccuracies and external disturbances are planned to be discussed in future publications of the authors.

The simulation environment, which was used for the here presented controller's robustness assessment, was modified in a way that multiplicative parameter uncertainties in the form of Eq. 20 could be considered.

$$C_{i,j} = \Delta C_{i,j}(\kappa_{i,j}) \cdot C_{i,j,nom} \qquad (20)$$

$$\Delta C_{i,j}(\kappa_{i,j}) = \mathcal{N}(1, (\frac{\kappa_{i,j}}{3})^2) \qquad (21)$$

For each as uncertain defined parameter $C_{i,j}$ a maximum uncertainty spreading $\kappa_{i,j}$ around the nominal value $C_{i,j,nom}$ was defined. In the current project state, the uncertainty distribution's probability density function (PDF) is invariably assumed as a Gaussian normal distribution. In later stages of the research activities also other PDFs are planned to be added to the framework. As Eq. 21 shows, is the considered uncertainty distribution factor $\Delta C_{i,j}$ defined so that the maximum occurring parameter deviation will generally lie within a range of $\pm 3\sigma$ standard deviation around $C_{i,j,nom}$. Regarding the here presented results of the controller's robustness assessment, for each uncertain parameter $C_{i,j}$, a new sample value of the parameter deviation was computed for every simulation run.

Table 1 presents the selected parameters and uncertainty spreading for the discussed robustness assessment of the proposed controller. The addressed parameter selection and uncertainty definition are based on prior project experiences and parameter variation studies on the regarded flight dynamical ve-

Table 1 Chosen uncertainty parameter properties of the conducted robustness analysis of the proposed control architecture.

Aerodynamic coefficient uncertainties	
Uncertaint parameter $C_{i,j}$	Uncertainty spreading $\kappa_{i,j}$
$C_{m,\alpha}$	10 %
$C_{m,\delta_{UL}}$	30 %
$C_{m,\delta_{UR}}$	30 %
$C_{m,\delta_{LL}}$	30 %
$C_{m,\delta_{LR}}$	30 %

hicle characteristics. For the discussed assessment, the flight vehicle was trimmed within the hypersonic speed regime and at a height band within the mesosphere. The results for the assessment of the nominal model are shown in Fig. 5. The doublet reference command on α_{cmd} is shown in black, and the response of the vehicle is displayed in red.

It can be seen that the proposed controller adequately and smoothly tracks the delivered raw trajectory on the angle-of-attack channel with the desired response characteristics defined in the RM. Since no raw pitch rate command is given to the system, the shown shaped reference signal of the normalized pitch rate is computed using the $\dot{\alpha}_{ref}$ command of the RM. In order to compare it with a pitch rate in the body-fixed axis, it was priorly transformed using the relationship presented in Eq. 10. The vehicle's normalized pitch rate closed-loop response follows the desired system behavior well and shows beneficial damping characteristics of the inner loop controllers. Further in-depth analysis and observations of the simulation have shown that the a priori assumed system's timescale separation is valid due to significant bandwidth differences between the inner and outer loop controllers. The time series of the fin deflection shows that, for a pure longitudinal maneuver, the deflections are symmetric on the left and right sides, but contrary on the upper and lower sides. It can be further observed that in order to maintain the regarded trimmed flight point, the upper fins are already occupied by around 58 %. The trajectory can still be followed by only allocating 5 % additional deflections in the critical direction on both upper fins. However, further investigations on the regarded flight point need to be conducted to evaluate if a control deflection reserve of around 40 % conflicts with higher-level missions requirements. Such investigation does not need to be carried out for the lower flaps since both only need 8 % of the available deflection range and hence got more than enough reserves for more challenging maneuvers. The results for the assessment of the model, under the presence of parameter uncertainties, are shown in Fig. 6. The doublet reference command on α_{cmd} is shown in black, the response of the vehicle under the presence of uncertainties is displayed in blue, and the response of the nominal vehicle is presented in red. For the discussed robustness investigation, a Monte-Carlo simulation-based analysis run with 1000 samples was conducted.

It can be seen that the proposed controller shows good and robust tracking performance even under the presence of significant aerodynamical parameter uncertainties. This indicates that the proposed control structure is, even without the application of adaptive or robust control algorithms, able to cope with the defined model uncertainties.The normalized pitch rate and the angle-of-attack reponses of the vehicle are almost unaffected by the parameter uncertainties. The same can be observed for the fin deflections. The control effector occupation in the case with uncertainties is slightly increased. The deflections just increased in the extreme cases by around 1 % for both upper and lower flaps. This indicates that the considered uncertainties are not critical with regard to the control authority of the vehicle.

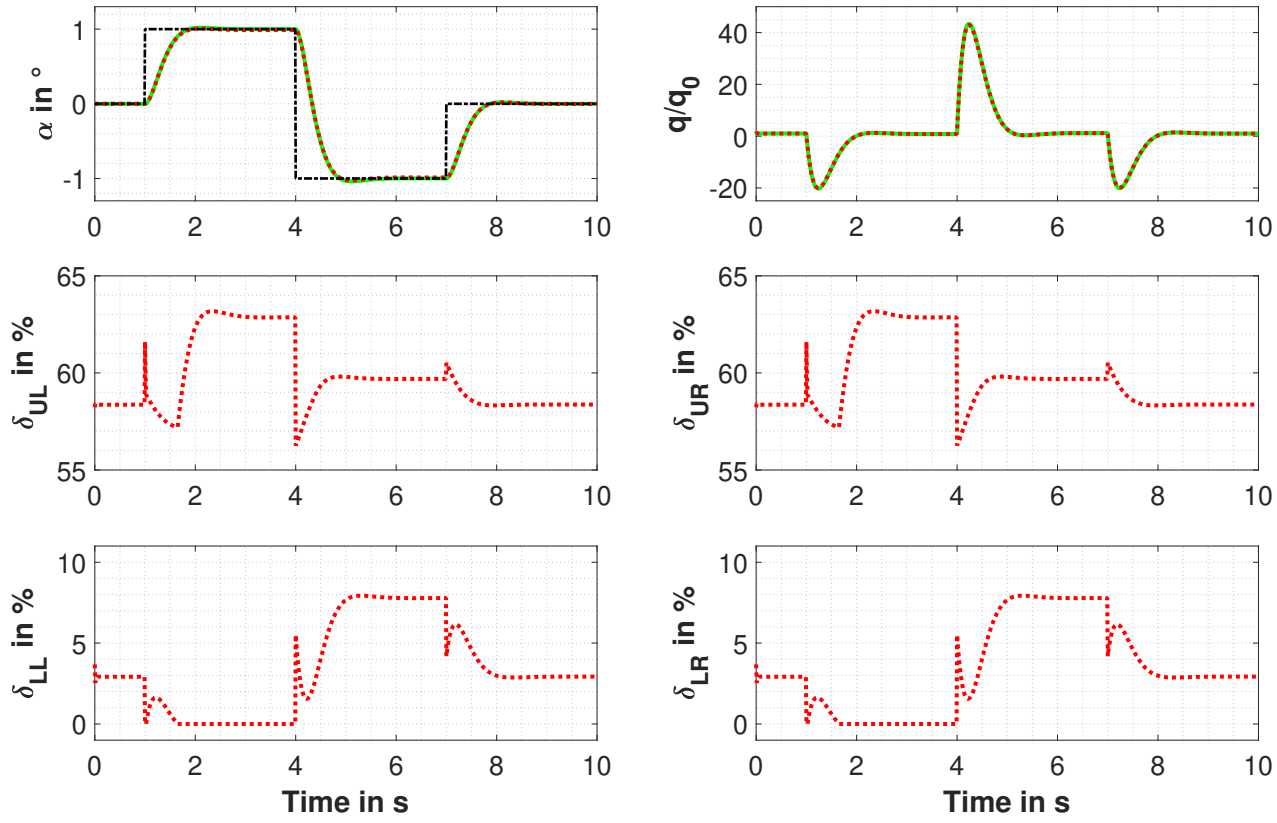

Fig. 5 Simulation results for a doublet command input on α_{cmd} in the case with no model uncertainties. Displayed time series: angle of attack α, normalized pitch rate and fin deflections in %. Black: raw reference command, green: shaped reference signal, red: vehicle response

5 Conclusions

This paper presents a nonlinear model following control architecture for the attitude control of an over-actuated conceptual hypersonic glide vehicle developed by DLR. The proposed flight control architecture applies a nonlinear dynamic inversion control methodology for feedback control and enhances the structures with a feedforward path based on the idea of nonlinear model following control. The methodology allows to partially seperate the command tracking tasks from the regulation tasks of the feedback control system and hence eases up the tuning and consequently decreases the possibility of high-gain solutions. The performance of the proposed control architecture was investigated in Sect. 4 with longitudinal maneuvers for the nominal case and under the presence of aerodynamical uncertainties. It was demonstrated that the proposed system handles the regarded system dynamics adequately in both investigated cases and provides good and robust tracking performance.

Even though the controller showed sufficient tracking and robustness properties within the investigated cases, as discussed in Sect. 4, further robustness assessments regarding regarding the influence of sensor errors and external disturbances need to be conducted to get better insights into the robustness properties of the proposed control architecture. Additionally, it is planned to improve the presented control architecture concerning mitigation of higher model deviations, such as actuator problems and control surface defects. Therefore it is considered to enhance the proposed control architecture with other modern control algorithms, such as adaptive control and fault detection, isolation, and recovery functionalities.

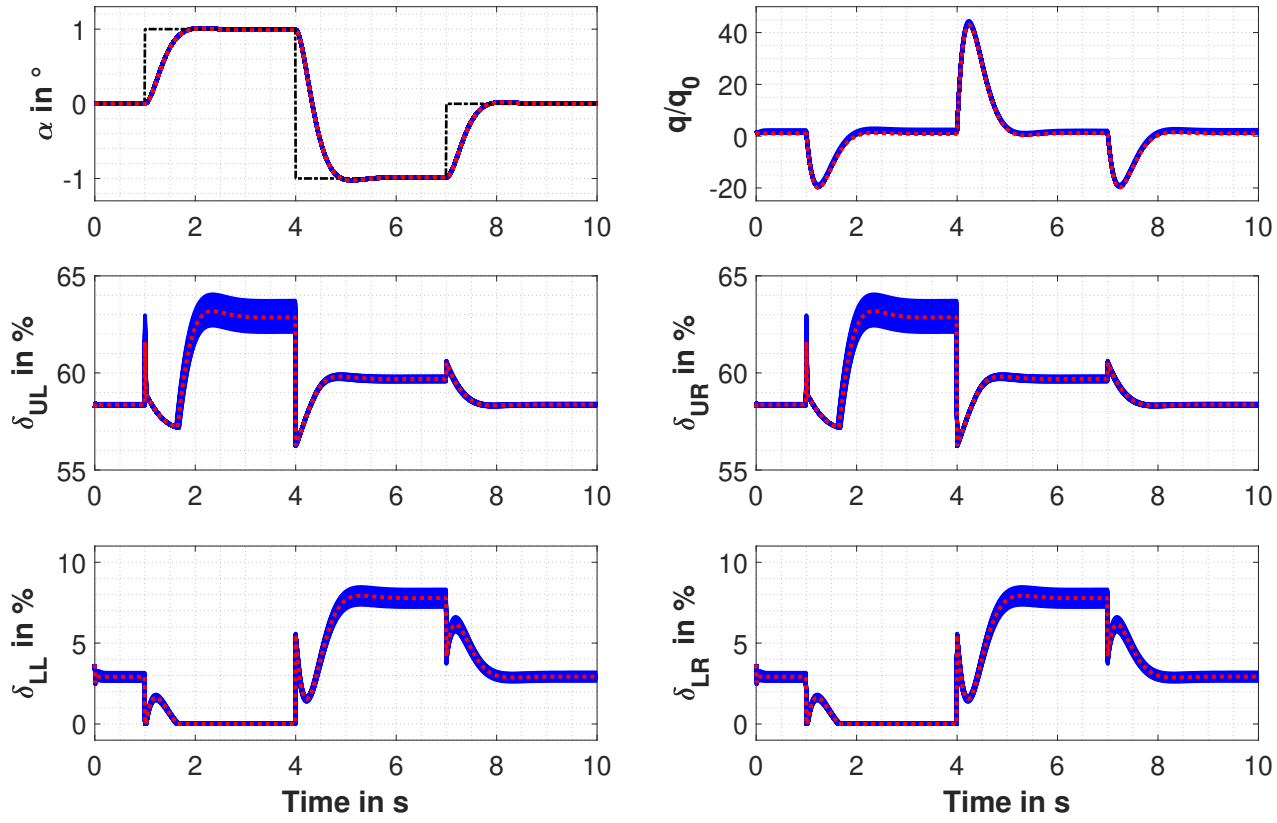

Fig. 6 Simulation results for a doublet command input on α_{cmd} in the case with model uncertainties. Displayed time series: angle of attack α, normalized pitch rate and fin deflections in %. Black: reference command, blue: uncertain vehicle response, red: nominal vehicle response

Acknowledgements

The authors would like to thank and acknowledge all colleagues from DLR working within the HyBAB study for their contributions to the multidisciplinary design of the discussed vehicle. Special thanks go to Dr. Patrick Gruhn from the DLR Institute of Aerodynamics and Flow Technology for helpful discussions and for supporting the vehicle's high-fidelity modeling. Further, the authors would like to thank Mr. Daniel Kiehn and Mr. Wulf Mönnich from the DLR Institute of Flight Systems for fruitful conversations and suggestions within the field of flight dynamics and control.

References

[1] International Organization for Standardization (ISO). Flight dynamics – Concepts, quantities and symbols – Part 1: Aircraft motion relative to the air. Standard, Geneva, Switzerland, April 1988. ISO 1151-1:1988.

[2] International Organization for Standardization (ISO). Flight dynamics – Concepts, quantities and symbols – Part 2: Motions of the aircraft and the atmosphere relative to the Earth. Standard, Geneva, Switzerland, September 1985. ISO 1151-2:1985.

[3] R. R. da Costa, Q. P. Chu, and J. A. Mulder. Reentry Flight Controller Design Using Nonlinear Dynamic Inversion. *Journal of Spacecraft and Rockets*, 40(1):64–71, January 2003. DOI: 10.2514/2.3916.

[4] S. A. Snell, F. D. Enns, and W. L. Garrard. Nonlinear Inversion Flight Control for a Supermaneuverable Aircraft. *Journal of Guidance, Control, and Dynamics*, 15(4):976–984, May 1992. DOI: 10.2514/3.20932.

[5] P. K. Menon, V. Iragavarapu, and E. Ohlmeyer. Nonlinear missile autopilot design using time-scale separation. August 1997. DOI: 10.2514/6.1997-3765.

[6] H. Duda, G. Bouwer, J.-M. Bauschat, and K.-U. Hahn. *A model following control approach*, pages 116–124. December 2007. DOI: 10.1007/BFb0113855.

[7] P. Gruhn. Design and Analysis of a Hypersonic Glide Vehicle (Original German Title: Auslegung und Analyse eines hypersonischen Gleitflugkörpers). In *Conference on Applied Research for Defense and Security in Germany*, Bonn, Germany, March 2020.

[8] N. Fezans, D. Alazard, N. Imbert, and B. Carpentier. *Robust LPV Control Design for a RLV During Reentry*. August 2010. DOI: 10.2514/6.2010-8194.

[9] D. Kiehn. Stability Analysis and Flight Control Design of the Winged Reusable Launch Vehicle ReFEx. *CEAS Space Journal*, 13:51–64, June 2020. DOI: 10.1007/s12567-020-00319-3.

[10] J. Autenrieb, N. Fezans, P. Gruhn, and J. Klevanski. Towards a Control-Centric Modelling and Simulation-Framework for Hypersonic Glide Vehicles. In *German Aeronautics and Space Congress (DLRK)*, Bremen, Germany, September 2021.

[11] O. Härkegård. *Backstepping and control allocation with applications to flight control*. PhD thesis, Linköpings universitet, Linköping, Sweden, April 2003.

[12] O. Härkegård. Dynamic control allocation using constrained quadratic programming. *Journal of Guidance Control and Dynamics*, 27(6), March 2004. DOI: 10.2514/1.11607.

[13] M. Bolender and D. Doman. Nonlinear Longitudinal Dynamical Model of an Air-Breathing Hypersonic Vehicle. *Journal of Spacecraft and Rockets*, 44:374–387, February 2007. DOI: 10.2514/1.23370.

[14] C. Breitsamter, T. Cvrlje, B. Laschka, M. Heller, and G. Sachs. Lateral-directional coupling and unsteady aerodynamic effects of hypersonic vehicles. *Journal of Spacecraft and Rockets*, 38(2):159–167, May 2001. DOI: 10.2514/2.3689.